Synchrotron XRF analyses of element distribution in fossilized sauropod dinosaur bones

M. Dumont
Max-Planck-Institut für Eisenforschung GmbH, Max-Planck-Straße 1, D-40237 Düsseldorf, Germany

N. Zoeger, C. Streli, and P. Wobrauschek
Atomic Institute of the Austrian Universities, Stadionallee 2, A-1020 Wien, Austria

G. Falkenberg
Hamburger Synchrotronstrahlungslabor HASYLAB at the Deutschen Elektronen-Synchrotron, DESY, Notkestrasse 85, D-22603 Hamburg, Germany

P. M. Sander
Institute of Palaeontology, University of Bonn, Nussallee, D-53115 Bonn, Germany

A. R. Pyzalla
Helmholtz-Zentrum Berlin, Glienicker Strasse 100, 14109 Berlin, Germany

(Received 30 September 2008; accepted 20 January 2009)

Sauropod dinosaurs were typically one magnitude larger than any other living or extinct terrestrial animal. This sheer size of the sauropod leads to scale effects in their biology and physiology that still are inadequately understood. The only remnants of the sauropods are their fossilized bones. These fossilized bones have sustained burial for some hundred million years and thus may have experienced significant diagenetic changes. These diagenetic changes often do not affect bone preservation on the histological level, but may lead to significant alterations of the bone microstructure. Here the influence of diagenesis on the microstructure of fossilized sauropod bones using femur cross section of *Brachiosaurus brancai* that was excavated in the Tendaguru beds in Tanzania is investigated. The element distribution in this dinosaur bone is studied by a combination of micro-X-ray-fluorescence (μ-XRF) using synchrotron radiation and energy dispersive X-ray analyses (EDX) in the scanning electron microscope. These techniques reveal quantitative values of the element concentration at a macroscopic level combined with qualitative information at high spatial resolution of the distribution of Ca, Co, Cr, V, Pb, U, Sr, Y, and As in the fossil bones. This allows a differentiation between the remnants of the original bone apatite and pore filling minerals and also a visualization of damage, e.g., cracks introduced by diagenetic processes. © *2009 International Centre for Diffraction Data.* [DOI: 10.1154/1.3131803]

Key words: XRF, synchrotron, diagenesis, sauropod dinosaurs

I. INTRODUCTION

Fossilized bones are the only remnants of sauropod dinosaur cadavers that are available today to provide information about their organism. Diagenesis (Karkanas *et al.*, 2000), which is the alteration of the bone that appears during burial and fossilization, may affect bone histology, bone porosity, protein content, the crystallinity of the bone apatite, carbonate content, and the bone's content of chemical species in general. The extent of diagenesis mainly depends on direct environmental conditions such as groundwater and sediment composition, soil hydrology and pH, redox potential and temperature, mechanical pressure, biological factors, and particle transport (Reiche *et al.*, 2003). During bone fossilization apatite replaces the structural protein collagen. The new apatite is incorporated into the bone by external Ca and P, which are transported into the bone via diffusion processes (Pfretzschner, 2000). While μm-scale structures of the bone often appear well preserved, early diagenetic pseudomorphosis of bone apatite crystallites can impede the recovery of *in vivo* compositional, trace element, and isotope data from fossil bone (Kolodny *et al.*, 1996; Hubert *et al.*, 1996). Different experimental approaches have been applied to studying and identifying diagenetic processes (Elliot and Grimes *et al.*, 1996). Chemical analyses and atomic absorption spectroscopy allow the determination of Sr and Ba (Samoilov and Benjamin, 1996), but they have the disadvantages of being destructive and offering at best a coarse spatial resolution. Electron probe microanalyses offer a spatial resolution in the μm and sub-μm range, but suffer from low sensitivity for elements such as Sr, U, Ba, and Zn, which are often encountered in fossilized bones (Elliot and Grime, 1993; Tükten *et al.*, 2004). X-ray microfluorescence (μ-XRF) analyses are nondestructive. They allow semiquantitative mapping of elements ($Z > 14$) with a local resolution in the order of some μm (depending on the X-ray optics in use) and have been frequently used for studies of archeological bones (Carvalho *et al.*, 2004). While most research on diagenetic effects on bone has been conducted on archeological bones, which typically are fully mineralised, here the elemental distribution is investigated in fossil sauropod dinosaurs buried roughly 140 to 150 million years ago (Romer, 2001). Using energy dispersive X-ray analyses in the SEM and μ-XRF, the distribution of chemical elements in the fossilized bones is studied with high local resolution. The aim of the combination of these methods is an assessment of the diagenetic effects in

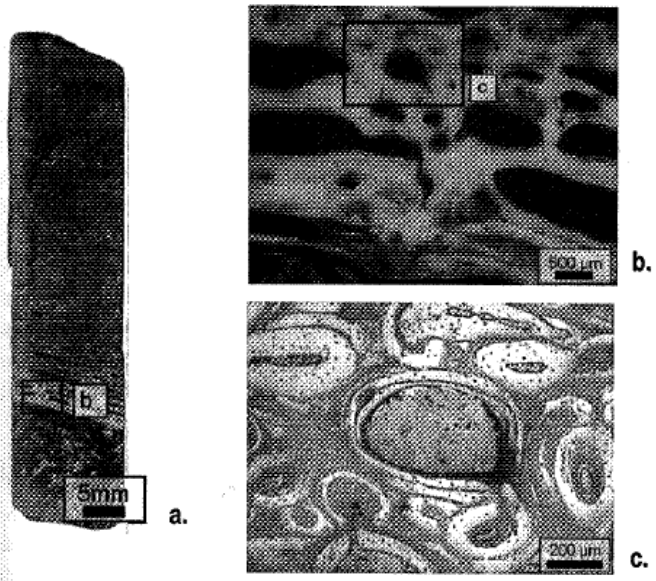

Figure 1. (Color online) Optical micrographs of the sample (BrXV, *Brachiosaurus brancai*, mature individual, femur, femur length 219 cm) (a). Overview of the bone cortex. [(b) and (c)] Closer view of the area of interest.

sauropod long bones both on a macroscopic and a microscopic scale.

II. EXPERIMENTAL

A. Sampling

This investigation focuses on sauropod long bones, mainly because they have an exceedingly simple morphology that is largely the product of appositional growth (Sander, 2000) and also because they are by far the most abundant in the famed Tendaguru sauropod fauna from Africa from Upper Jurassic (Romer, 2001), which today is housed in the *Museum für Naturkunde* of the Humboldt-Universität Berlin NHUB (Janensch, 1914; Janensch, 1950; Janensch, 1961; Heinrich, 1999). 15 mm diameter cores were drilled from the narrowest part of the diaphysis with details provided in Sander, 2000. Afterwards the cores were cut in half along their longitudinal axis. The specimens obtained are half-cylinders that cover the whole bone cortex from the cancellous bone in the center to the primary fibrolamellar bone on the outside. For the analyses, the half core was grinded using SiC paper, polished using diamond paste (1 μm size) on felt plate. The sample was then cleaned with alcohol. We started our analysis of the element composition of the sauropod fossil bones by choosing a core taken from specimen no. BrXV, which is a left femur of *Brachiosaurus brancai*, 219 cm in length (Janensch, 1961), excavated from the Tendaguru beds. Based on palaeohistological studies (Sander, 2000), the femur BrXV belonged to an individual that was still growing. Figure 1 gives an overview of this long bone cortex. The area investigated is located in the white part, between the cancellous bone and the periosteal bone. In this area, the Haversian system, lamellae, and canaliculi appear well preserved [Figure 1(c)].

1. Energy dispersive X-ray analyses in the scanning electron microscope (SEM-EDX)

SEM/EDX investigations were carried out on Philips XL30 tungsten filament electron microscope operating at 15 kV and equipped with EDAX EDS system. The EDX analyses were performed on uncoated samples. After the EDX analyses a thin gold layer was sputtered onto the sample surface in order to improve the quality of the secondary electron (SE) and the backscattered electron images (BSE). The element distribution maps obtained by EDX in the SEM reveal the element distribution in a qualitative way: the brighter an area appears in a map for a specific element, the higher is the element concentration.

2. Synchrotron micro-X-ray fluorescence analysis (μ-XRF)

Synchrotron radiation induced micro-X-ray fluorescence analysis (SR-μ-XRF) in confocal geometry was carried out at the micro focus end-station at HASYLAB, beamline L, Hamburg, Germany (Janssens *et al.*, 2004). The primary X-ray beam was monochromatized at 17 keV by a Ni/C multilayer monochromator and focused by a polycapillary half-lens onto the sample. A second polycapillary half-lens was installed in front of a silicon drift detector (SDD) in order to realize the confocal measurement geometry. By overlapping the focal spots of the two X-ray optic elements a well defined microvolume was achieved from which the fluorescence radiation was detected. Scanning a 4 μm thick Au foil and a 4 μm wire, the detection volume at an energy of the Au-$L\alpha$ line (9.7 keV) was determined to be $20 \times 14 \times 22$ μm^3 (lateral $\times$ height $\times$ depth). In the present experiment the 3D capabilities of confocal SR-μXRF were exploited to inhibit unwanted contribution of deeper sample layers (sample thickness $\sim$5 mm) to the X-ray fluorescence spectra. In order to enable a comparison of the XRF results with data from the other imaging techniques a confocal μ-XRF area scan was performed in the first layer of the sample. Fluorescence spectra were recorded at 68×46 pixels using a step size of 10 μm in each direction and a counting time of 5 s per pixel. Net intensities for each pixel were obtained by AXIL fitting [AXIL Tools in QXAS version by IAEA, (Vekemans *et al.*, 1994)] and normalization to 100 mA ring current and correction for detector dead time. Element maps were generated by converting the intensity data to 8-bit grayscale images using a scaling from 0 (black) to the maximum counts (white) for each detected element.

III. RESULTS

A. EDX analysis in the scanning electron microscope

The topographic features visible in the scanning electron microscope (SEM) image are visible also in the EDX maps of Ca, C, Mg, Na, P, Si, and O (Figure 2). The vascular canal contains a higher Ca, C, and O concentration than the fossil bone tissue [the bone tissue originally consisted of hydroxyapatite $Ca_{10}(PO_4)_6(OH)_2$]. It reveals the presence of calcium carbonate $CaCO_3$ in the vascular canal. In contrast, the fossil bone apatite contains more P, Si, Mg, and Na than the vascular canal. Since P was not detected in the calcium carbonate, the P distribution reveals very clearly the remnants of the

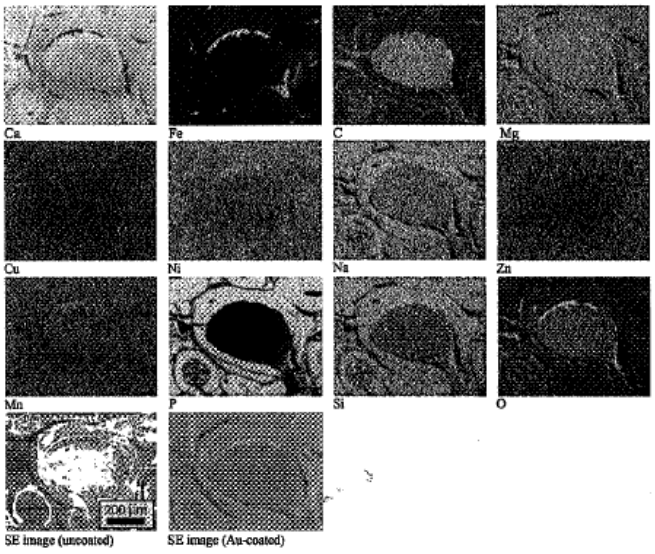

Figure 2. SEM EDX element distribution maps of area of interest.

apatite. Thus, the dark areas in the P EDX map reveal details such as cracks introduced by diagenetic processes, e.g., in the lamellae surrounding the vascular canal.

Comparing the P, Ca, and Fe EDX maps reveals Fe enrichment at the interface between the vascular canal and the former apatite. In these areas with high iron content, both Ca and P contents are low. The Fe enrichment is accompanied by a substantial O enrichment, revealing the formation of iron oxides in these spaces. Also the Si, Mn, and Ni contents are higher in these regions than within the calcium carbonate and the formed apatite.

B. SR-μ-X-ray fluorescence analysis (SR-μ-XRF)

The element distribution maps obtained with high spatial resolution using synchrotron radiation μ-XRF similar to the EDX analyses in the SEM reveal a qualitative image of the element distribution (Figure 3). For each element a scaling was performed with respect to the minimum and the maximum intensities obtained in the spectra collected over the sampled area. The dark areas in the plots for each element correspond to regions where we measured low XRF intensities, on the contrary an increasing brightness corresponds to higher intensities in the XRF spectra and thus to an enrichment in the respective element. Besides element distribution maps obtained for Ca, Fe, Cu, Ni, Zn, and Mn, where SEM EDX maps could be measured, μ-XRF maps were determined for Co, Cr, V, Pb, U, Sr, Y, and As. Even more clearly than the EDX maps the μ-XRF maps show the Ca distribution and thus the localization of the calcium carbonate within the vascular canal of the bone, in the cracks and between different lamellae surrounding the vascular canal. The calcium carbonate in addition to Ca, C, and O only contains Mn and a low amount of Sr. Compared to the calcium carbonate the former apatite contains a significantly higher Sr concentration. The μ-XRF distribution map of Sr in the former apatite compares well with the U distribution. The Zn distribution in the former apatite also appears similar to the Sr and U distribution. In both the U and the Sr map the calcium carbonate filled crack and the calcium carbonate filled rims between the lamellae are visible, which were also observed in the SEM EDX maps. Fe, Co, Cr, Cu, Ni, V, Zn, Mn, Pb, and As show relative maximum values in the same locations at the interface between the calcium carbonate and the former apatite. The local maximum values of the Fe concentration determined by μ-XRF coincide with those determined by SEM-EDX.

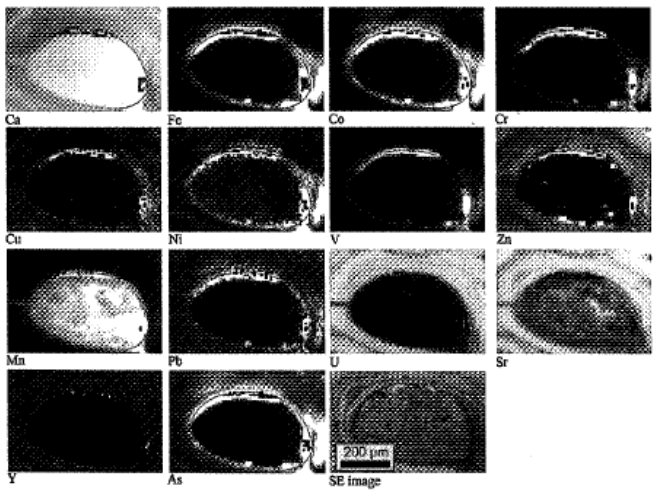

Figure 3. (Color online) μ-XRF element distribution maps of area of interest.

IV. DISCUSSION

A. EDX analysis in the SEM

This technique is a fast and far more easily accessible tool for semiquantitative analyses (C, O, and other light elements cannot be quantified reliably. However, this drawback can be overcome using WDX analysis in a microprobe SEM) at the sample surface. By mapping the X-ray intensity of various chemical elements, their distribution can be related to the fossil microstructure. The EDX maps of the P distribution directly reveal radial microcracks in the lamellae of the former vascular canals. The formation of radial microcracks can be attributed to diagenetic processes (Behrensmeyer, 1978). The microcracks form early during diagenesis due to internal stresses during the replacement of collagen by apatite (Pfretzschner, 2000). The radial microcracks according to (Bell, 1990; Pfretzschner, 2000) have an important role during the diagenetic process, since they open additional pathways for diffusion in the Haversian bone and thus they contribute significantly to recrystallization and crystal growth of the former hydroxyapatite in the bone. In addition to radial microcracks, polygonal crack networks are also visible in the EDX map of the element P. These polygonal cracks supposedly appear later during the diagenetic process due to external pressure on the fossil (Pfretzschner, 2000).

B. Synchrotron μ-XRF analysis

Synchrotron μ-XRF analysis was first applied for the characterization of the element distribution in fossil bones. It provides a map of the element distribution with a spatial resolution comparable to those offered by EDX in the SEM, but due to its higher detection level in the order of a few

ppm, the distribution of elements such as U, Sr, Pb, and As can be determined, which are of particular interest for dietary indicators (Parker and Toots, 1980; Ezzo, 1994; Rheingold *et al.*, 1983; Safont *et al.*, 1998). Compared to XRF using laboratory X-ray sources (Ferreyro *et al.*, 2006) synchrotron μ-XRF provides a substantially higher spatial resolution and lower detection limits (in the range of ng/g). The combination of synchrotron XRF analyses with EDX analyses in the SEM provides a very clear differentiation between original and diagenetically formed apatite and pore-filling minerals such as calcium carbonate or iron oxides, because P as well as U and Sr as minerals with an affinity to bone are almost exclusively present in the apatite.

C. Element distribution in sauropod dinosaur bones

A comparison of the element concentrations in the sauropod bone fossils basically indicates agreement with earlier investigations on archeological bones (Lambert *et al.*, 1985; Reiche *et al.*, 2003), showing that Ca, Na, K, and Pb are lower in the excavated samples (they leach out) and Fe, Mn, and Al are enriched in the excavated samples. Except for Fe, on a macroscopic level the distribution of elements in the sauropod bone investigated appears fairly homogeneous. Fe, Mn: Compared to modern bone, the fossilized sauropod femur shows a significantly higher Fe and Mn content. Both the SEM-EDX and the μ-XRF element maps show that Fe and Mn apparently have a very similar spatial distribution, and a similar correlation of Fe and Mn was shown by PIXE microprobe investigations of archeological human bones (Boscher-Barre *et al.*, 1992). Elliott and Grime (Elliott and Grime, 1993) found Mn concentrated within the bone in patterns that correspond to the bone's small pore and canaliculi structures while Fe more typically filled the larger pores in the bone matrix such as Haversian canals. The combined occurrence of Fe, Mn, Cr, V, Si, and O in the fossilized sauropod bones reveals that an oxide seam formed at the interface between the vascular canals and the former hydroxyapatite. Mn, besides being incorporated into the oxides, is known as a contaminant of the calcium carbonate from soil solution (Reeder *et al.*, 1987). Enrichment of Fe in fossil bones has been observed previously by Lambert *et al.* and Karkanas *et al.* (Lambert *et al.*, 1985 and Karkanas *et al.*, 2000). The distribution of Fe, which mainly covers the inner surface of the voids created by the degeneration of organic parts, might indicate that the iron oxides formed at an early stage of the diagenetic process. Sr, U: Sr and U are two elements incorporated in the hydroxyapatite. Sr substitutes Ca in hydroxyapatite (Parker and Toots, 1980) and thus is mainly present in the fossilized former hydroxyapatite, but not exclusively present as earlier reported by (Ezzo, 1994). U is incorporated into the bone as complexes of the Uranyl ion by diffusion and subsequent adsorption (Millard and Hedges, 1985). The U decrease toward the medullar cavity might indicate that part of it leached out during the diagenetic process. Mg, Na: Light chemical species such as Mg and Na appear to be homogeneously distributed within the fossilised bone in contrast to previous studies on archeological bones where Mg and Na were shown to leach out of the bone (Parker and Toots, 1980; Reiche *et al.*, 2003). This homogeneous distribution is attributed to the long time available for diffusion. Ca: According to Karkanas *et al.*, 2000, in the presence of calcium carbonate the pH of the bones is controlled by the pH of the waters entering the bone, which in turn prevents the dahllite from being dissolved. Thus the incorporation of large amounts of calcium carbonate in the sauropod fossil bones is an indication that most of the original apatite has been conserved.

V. CONCLUSIONS

μ-X-ray fluorescence analyses using synchrotron radiation determined the preferential location of elements within the sauropod fossils. The analyses allowed a qualitative determination of the element distribution on the level of a few 100 μm^2. Additional EDX analyses in the SEM provided information about the distribution of lower Z elements. The combination of the different analysis techniques revealed that although seemingly unaffected at the histological level, the sauropod fossils endured strong diagenetic changes. Element maps of P obtained by SEM and element maps of Sr and U obtained by μ-XRF reveal the location of the remnants of the sauropod bone and show microcracks introduced by diagenesis. Both methods show that diagenetic minerals filled these microcracks and also the vascular canals of the bones. The concentration and distribution of the trace elements in the sauropod bones reveals that even in case of these extraordinary large fossils strong diagenetic changes occurred, which render conclusions about the abundance of trace elements in the living bones of sauropods extremely difficult.

ACKNOWLEDGMENTS

We gratefully acknowledge the support of Ing. C. Zaruba, TU Wien and HASYLAB, Hamburg, for providing beam time and experimental support at station L1. This work was supported by the "European Community Research Infrastructure Action" in the FP6 "Structuring the European Research Area" Program. Author P.M.S. acknowledges financial support within the framework of the research unit "Sauropod Biology–Evolution of Gigantism" by the Deutsche Forschungsgemeinschaft (DFG). This is contribution no. 28 of this research unit.

Behrensemeyer, A. K. (**1978**). "Taphonomic and ecologic information from bone weathering," Paleobiology **4**, 150–162.

Bell, L. S. (**1990**). "Palaeopathology and diagenesis: An SEM evaluation of structural changes using backscattered electron imaging," J. Archaeol. Sci. **17**, 85–102.

Boscher-Barre, N., Trocellier, P., Deschamps, N., Dardenne, C., Blondiaux, J., and Buchet, L. (**1992**). "Nuclear micropore study of trace element in archeological bones," J. Trace Microprobe Tech. **10**, 77–90.

Carvalho, M. L., Marques, A. F., Lima, M. T., and Reus, U. (**2004**). "Trace elements distribution and post-mortem intake in human bones from Middle Age by total reflection X-ray fluorescence," Spectrochim. Acta, B At. Spectrosc. **59**, 1251–1257.

Elliott, T. A. and Grime, G. W. (**1993**). "Examining the diagenetic alteration of human bone material from a range of archaeological burial sites using nuclear microscopy," Nucl. Instrum. Methods Phys. Res. B **77**, 537–547.

Ezzo, J. A. (**1994**). "Putting the chemistry back into archaeological bone chemistry analysis: Modeling potential paleodietary indicators," J. Anthropol. Archaeol. **13**, 1–34.

Ferreyro, R., Zoeger, N., Cernohlawek, N., Jokubonis, C., Koch, A., Streli, C., Wobrauschek, P., Sander, P. M., and Pyzalla, A. (**2006**). "Determi-

nation of the element distribution in sauropod long bones by micro-XRF," Adv. X-Ray Anal. **49**, 230–235.

Heinrich, W.-D. (**1999**). "The taphonomy of dinosaurs from the Upper Jurassic of Tendaguru, Tanzania (East Africa), based on field sketches of the German Tendaguru expedition (1909–1913)," Mitteilungen aus dem Museum für Naturkunde in Berlin, Geowissenschaftliche Reihe **2**, 25–61.

Hubert, J. F., Parish, P. T., Chure, D. J., and Prostak, K. S. (**1996**). "Chemistry, microstructure, petrology, and diagenetic model of Jurassic dinosaur bones, Dinosaur National Monument, Utah," J. Sediment. Res. **66**, 531–547.

Janensch, W. (**1914**). "Übersicht über die Wirbeltierfauna der Tendaguruschichten, nebst einer kurzen Charakterisierung der neu aufgeführten Arten von Sauropoden," Archiv für Biontologie **3**, 81–110.

Janensch, W. (**1950**). "Die Skelettrekonstruktion von *Brachiosaurus brancai*," Palaeontographica **7**, 97–103.

Janensch, W. (**1961**). "Die gliedmaszen und gliedmaszengürtel der sauropoden der Tendaguru-Schichten," Palaeontographica **7**, 177–235.

Janssens, K., Proost, K., and Falkenberg, G. (**2004**). "Confocal microscopic X-ray fluorescence at the HASYLAB microfocus beamline: Characteristics and possibilities," Spectrochim. Acta, Part B **59**, 1637–1645.

Karkanas, P., Bar-Yosef, O., Goldberg, P., and Weiner, S. (**2000**). "Diagenesis in prehistoric caves: The use of minerals that form *in situ* to assess the completeness of the archaeological record," J. Archaeol. Sci. **27**, 915–929.

Kolodny, Y., Luz, B., Sander, M., and Clemens, W. A. (**1996**). "Dinosaur bones: fossils or pseudomorphs? The pitfalls of physiology reconstruction from apatitic fossils," Palaeogeogr. Palaeoclimatol. Palaeoecol. **126**, 161–171.

Lambert, J. B., Vlasak Simpson, S., Szpunar, C. B., and Buikstra, J. E. (**1985**). "Bone diagenesis and dietary analysis," J. Hum. Evol. **14**, 477–482.

Millard, A. R. and Hedges, R. E. M. (**1995**). "The role of the environment in uranium uptake by buried bone," J. Archaeol. Sci. **22**, 239–250.

Parker, R. B. and Toots, H. (**1980**). *Fossils in the Making: Vertebrate Taphonomy and Paleoecology*, edited by Behrensmeyer, A. K. and Hill, A. P. (University of Chicago, Chicago), pp. 197–207.

Pfretzschner, H.-U. (**2000**). "Microcracks and fossilization of Haversian bone," Neues Jahrb. Mineral., Abh. **216**, 413–432.

Reeder, R. J. and Grams, J. C. (**1987**). "Sector zoning in calcite cement crystals: Implications for trace element distributions in carbonates," Geochim. Cosmochim. Acta **51**, 187–194.

Reiche, I., Favre-Quattropani, L., Vignaud, C., Bocherens, H., Charlet, L., and Menu, M. (**2003**). "A multi-analytical study of bone diagenesis: the Neolithic site of Bercy (Paris, France)," Meas. Sci. Technol. **14**, 1608–1619.

Rheingold, A. L., Hues, S., and Cohen, M. N. (**1983**). "Strontium and zinc content in bones as an indication of diet," J. Chem. Educ. **60**, 233–234.

Romer, R. L. (**2001**). "Isotopically heterogeneous initial Pb and continuous ^{222}Rn loss in fossils: The U-Pb systematics of *Brachiosaurus brancai*," Geochim. Cosmochim. Acta **65**, 4201–4213.

Safont, S., Malgosa, A., Subira, M. E., and Gibert, J. (**1998**). "Can trace elements in fossils provide information about palaeodiet?" Int. J. Osteoarchaeol. **8**, 23–37.

Samoilov, V. and Benjamini, Ch. (**1996**). "Geochemical features of dinosaur remains from the Gobi Desert, South Mongolia," Palaios **11**, 519–531.

Sander, P. M. (**2000**). "Longbone histology of the Tendaguru sauropods: Implications for growth and biology," Paleobiology **26**, 466–488.

Tükten, T., Pfretzschner, H.-U., Vennemann, T. W., Sun, G., and Wang, Y. D. (**2004**). "Paleobiology and skeletochronology of Jurassic dinosaurs: Implications from the histology and oxygen isotope compositions of bones," Palaeogeogr. Palaeoclimatol. Palaeoecol. **206**, 217–238.

Vekemans, B., Janssens, K., Vincze, L., Adams, F., and Van Espen, P. (**1994**). "Analysis of X-ray spectra by iterative least squares (AXIL): New developments," XRay Spectrom. **23**, 278–285.